Available online at www.sciencedirect.com
ScienceDirect
Polymer 47 (2006) 7170–7177
polymer
www.elsevier.com/locate/polymer

Effect of pressure on the segmental dynamics of bisphenol-A-polycarbonate

K. Mpoukouvalas [a,b], N. Gomopoulos [a,b], G. Floudas [a,b,*], C. Herrmann [c], A. Hanewald [c], A. Best [c]

[a] University of Ioannina, Department of Physics, P.O. Box 1186, 451 10 Ioannina, Greece
[b] Foundation for Research and Technology-Hellas (FORTH), Biomedical Research Institute (BRI), Greece
[c] Max-Planck-Institut für Polymerforschung, D-55021 Mainz, Germany

Received 21 February 2006; received in revised form 28 April 2006; accepted 2 May 2006
Available online 30 June 2006

Dedicated to the memory of the scientist and friend Tadeusz Pakula.

Abstract

The segmental dynamics of bisphenol-A-polycarbonate (BPA-PC) are studied as a function of temperature (in the range from 143 to 473 K) and pressure (0.1–300 MPa) within the frequency range from 3×10^{-3} to 1×10^{6} Hz using dielectric spectroscopy aiming at extracting the more relevant parameter associated with the liquid-to-glass transition. Rheological measurements are also made in the temperature range from 408 to 513 K for comparison. The dynamic results coupled with the equation of state reveal that both density and thermal energy control the segmental dynamics with density being the most important variable in the vicinity of the transition. This is documented by independent estimates of the value of the dynamic ratio E_V^*/H^* ($\sim$0.44). This low value of the dynamic ratio is discussed in terms of the packing irregularities and large monomer volume of BPA-PC. In addition, the pressure coefficient of T_g ($dT_g/dP \sim 0.52$ K/MPa) is one of the highest for a polymeric substance.

Keywords: Bisphenol-A-polycarbonate; Glass transition; Pressure dependence

1. Introduction

Bisphenol-A-polycarbonate forms a glassy polymer notable for its high impact resistance and ductility over a broad temperature range. Molecular dynamics within the glassy state are thought to contribute to these favorable mechanical properties. Therefore there is an extensive literature on the origin of the low-temperature relaxation (known as γ-process) of BPA-PC [1–8].

On the other hand, the origin of the segmental motion is much less investigated. In addition, there exist several peculiarities in BPA-PC associated with longer length scales than the glassy γ-process. Both experiments and simulations show an increase of the static structure factor $S(q)$ at low values of the wavevector q, suggesting the existence of large-scale inhomogeneities [9]. Positron-annihilation-lifetime spectroscopy measurements (PALS) correlated with dilatometric measurements allowed an estimation of the fraction of free volume as well as the concentration of free-volume entities [10–12]. It was shown that BPA-PC is a defect-full polymer with a broad distribution of hole sizes. The fraction of free volume was estimated at about 8% at the glass temperature T_g [10]. Measurements of the rotational and translational diffusion of the probe molecule rubrene indicated that the segmental dynamics in BPA-PC are spatially heterogeneous with an enhanced translation by up to 3.5 orders of magnitude over the expected behavior for homogeneous dynamics [13]. Lastly and on a longer length scale, we mention the extraordinarily small value of the entanglement molecular weight ($M_e \sim$ 1200 g/mol, corresponding to about 5 monomer units) [14].

There exist two studies of the effect of hydrostatic pressure on the dynamics of BPA-PC. In the first such investigation the ^{1}H NMR linewidths were measured for temperatures up to 353 K and for pressures up to about 180 MPa [15]. The apparent activation volume was $\sim$25 cm^3/mol, i.e., about 10% of the

* Corresponding author. University of Ioannina, Department of Physics, P.O. Box 1186, 451 10 Ioannina, Greece. Tel.: +30 2651 098564; fax: +30 2651 098693.
E-mail address: gfloudas@cc.uoi.gr (G. Floudas).

0032-3861/$ - see front matter © 2006 Elsevier Ltd. All rights reserved.
doi:10.1016/j.polymer.2006.05.068

repeat-unit volume. This suggested that volume fluctuations of only one-fourth to one-third of that of a single phenylene ring of the repeat unit take place within the low-temperature γ-process as seen in NMR. In the second investigation the ^{2}H NMR spin-lattice relaxation was studied in the glassy state and for pressures up to 250 MPa [16]. The apparent activation volume was estimated at different temperatures and the small values suggested again that the molecular motions are highly restricted in the glassy state. Despite this, an increase in apparent activation volume was found with increasing temperature suggesting that phenylene motions become less restricted with increasing temperature.

Despite these important studies on the glassy dynamics, the segmental (α-) dynamics have not been investigated under pressure. Pressure (P) dependent measurements on the length scale of the segmental process are of paramount importance in addressing the origin of the liquid-to-glass transition [17–19]. Such measurements allow a quantitative measure of the relevant parameter controlling glass formation i.e., whether the dynamics are only controlled by density (or volume or "free" volume) as suggested by free-volume theories [20,21], or by temperature through the thermal energy k_BT, as suggested by different "landscape" models [22,23]. By changing the temperature alone, both thermal energy and density are changing, making impossible the separation of the two effects. In the present investigation we explore the origin of the liquid-to-glass transformation in BPA-PC by employing pressure-dependent dielectric spectroscopy (DS) measurements. The T- and P-dependent DS measurements combined with knowledge of the equation of state enable an investigation of the segmental dynamics under "iso-density" conditions. Under such conditions, the relative contributions from volume and thermal energy can be separately discussed, and the origin of the dynamic arrest at T_g can be clarified. We find a strong coupling between the static and dynamic properties; molecular packing and monomer volume play a central role in explaining the freezing of the segmental dynamics of BPA-PC at T_g.

2. Experimental section

2.1. Sample

The BPA-PC sample (Bayer) had $M_w = 30\,200$ g/mol and a polydispersity of $M_w/M_n = 2.9$. The glass-transition temperature was 420 K as determined by differential scanning calorimetry (DSC) at a heating rate of 10 K/min with heat capacity step, Δc_p, of $\Delta c_p = 0.25$ J/gK. Scheme 1 shows the repeat unit of BPA-PC.

2.2. Rheology

An advanced rheometric expansion system (ARES) equipped with a force-rebalanced transducer was used in the oscillatory mode. Depending on the temperature range two transducers were used with 2000, 2 g cm and 200, 0.2 g cm upper and lower sensitivities, respectively. The sample was

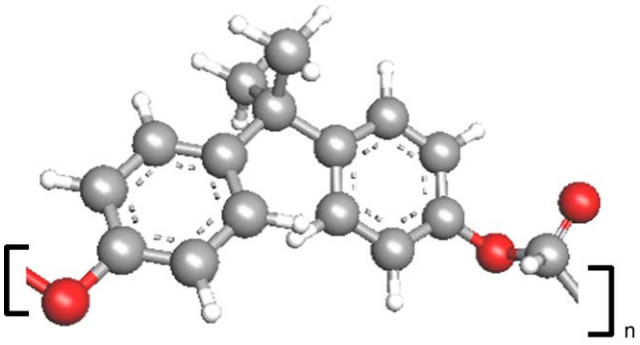

Scheme 1. Schematic representation of the repeat unit of BPA-PC.

prepared on the lower plate of the 6 mm diameter parallel plate geometry set-up and heated under a nitrogen atmosphere until it could flow. Subsequently, the upper plate was brought into contact, the gap thickness was adjusted to 1 mm, and the sample was slowly cooled to the desired starting temperature. The storage (G') and loss (G'') shear moduli were monitored in different types of experiments. First, the linear and nonlinear viscoelastic ranges were identified, by recording the strain amplitude dependence of the complex shear modulus $|G^*|$ at selected temperatures. In the subsequent experiments strain amplitudes within the linear viscoelastic range were used (typically below 0.5% except at 493 and 513 K where strain amplitudes of 2 and 4%, respectively, were necessary). These experiments involved isothermal frequency scans for temperatures in the range 408–513 K and for frequencies $10^{-2} < \omega < 10^2$ rad/s.

2.3. Wide-angle X-ray scattering (WAXS)

WAXS was made with a Siemens θ–θ diffractometer. The CuKα radiation was used with a secondary graphite monochromator from a Siemens generator (Kristalloflex 710H) operating at 35 kV and 30 mA. The measurements were made within the q range ($q = (4\pi/\lambda)\sin(2\theta/2)$, 2θ is the scattering angle) from 1 to 47 nm^{-1} at room temperature. The characteristic diffraction pattern is characterized by an intense peak at $q \sim 12$ nm^{-1}, known as the van der Waals peak [24], with a corresponding distance of 0.51 nm reflecting the average chain distance. Another shallow peak at $q \sim 6$ nm^{-1} is mainly caused by correlations between the carbonate groups and it is of intramolecular origin [9].

2.4. Dielectric spectroscopy

The sample cell consisted of two electrodes with 20 mm in diameter and the sample with a thickness of 50 μm maintained by Teflon spacers. The dielectric measurements were made at different temperatures in the range from 143 to 473 K, at atmospheric pressure, and for frequencies in the range from 3×10^{-3} to 1×10^6 Hz, using a Novocontrol BDS system composed from a frequency response analyzer (Solartron Schlumberger FRA 1260) and a broadband dielectric converter. In addition, pressure-dependent measurements were made under

"isothermal" conditions (the following temperatures were used: 443.15, 448.15, 453.15, 458.15, 463.15, 468.15, 473.15 K) and for pressures in the range from 0.1 to 300 MPa using the experimental set-up described elsewhere in detail, in steps of 10 MPa. Such small pressure increments were necessary in view of the strong $\tau_\alpha(P)$ dependence. The complex dielectric permittivity $\varepsilon^* = \varepsilon' - i\varepsilon''$, where ε' is the real and ε'' is the imaginary part, is a function of frequency ω, temperature T and pressure P, $\varepsilon^* = \varepsilon^*(\omega,T,P)$. In the analysis of the DS spectra we have used the empirical equation of Havriliak and Negami (HN):

$$\varepsilon^*(T,P,\omega) = \varepsilon_\infty(T,P) + \sum_j \frac{\Delta\varepsilon_j(T,P)}{\left[1+\left(i\omega\tau_{jHN}(T,P)\right)^{\alpha_j}\right]^{\gamma_j}} + \frac{\sigma_0(T,P)}{i\varepsilon_f\omega} \quad (1)$$

where $\varepsilon_\infty(T,P)$ is the high-frequency permittivity, $\tau_{HN}(T,P)$ is the characteristic relaxation time in this equation, $\Delta\varepsilon_j(T,P) = \varepsilon_o(T,P) - \varepsilon_\infty(T,P)$ is the relaxation strength of the jth relaxation mode, α_j, γ_j (with limits $0 < \alpha$, $\alpha\gamma \le 1$) describe, respectively, the symmetrical and asymmetrical broadening of the distribution of relaxation times, σ_0 is the dc-conductivity and ε_f is the permittivity of free space. From τ_{HN}, the relaxation time at maximum loss, τ_{max}, is obtained analytically following

$$\tau_{max} = \tau_{HN}\left[\frac{\sin\left(\frac{\pi\alpha}{2+2\gamma}\right)}{\sin\left(\frac{\pi\alpha\gamma}{2+2\gamma}\right)}\right]^{-1/\alpha} \quad (2)$$

The slow process was covered by the strong conductivity contribution making the direct analysis of the dielectric loss data ε'' a formidable task. In this case we have made use of the first derivative method of ε' to derive the ε'' as: $\varepsilon''_{calc} = -(\pi/2)(\partial\varepsilon'/\partial\ln\omega)$, which provides a conduction-free dielectric loss peak [25]. An alternative representation of the dielectric data is through the inverse of the dielectric function $\varepsilon^*(\omega)$ i.e., the electric modulus, related to the dielectric function through [26]

$$M^*(\omega) = \frac{1}{\varepsilon^*(\omega)} = M' + iM'' \quad (3)$$

where M' and M'' are the real and imaginary parts of the electric modulus, respectively. The electric modulus representation (i.e., the decay of the electric field under conditions of constant dielectric displacement, D) rather than the dielectric function (constant electric field, E) has been proposed not only for systems containing a substantial concentration of mobile carriers but also for any dielectrically active process. There are also cases where the use of $M^*(\omega)$ is an absolute necessity, as in the present case (i.e., comparison with rheology data). The relaxation times obtained from the electric modulus (τ_{M^*}) and the dielectric function (τ_{ε^*}) scale as $\tau_{M^*}/\tau_{\varepsilon^*} \sim \varepsilon_\infty/\varepsilon_s$ (exact equality only in the case of $\alpha = \gamma = 1$) and can differ substantially in systems with high dielectric strengths. Finally, the dipole moments corresponding to the α-process were calculated. The dielectric strength, $\Delta\varepsilon$, is directly related to the dipole moment through the equation $\Delta\varepsilon = (4\pi FNg\mu^2/3k_BT)$, where μ is the dipole moment, N is the number of dipoles per unit volume, $F = (\varepsilon_0(\varepsilon_\infty+2)^2/3(2\varepsilon_0+\varepsilon_\infty))$ is the local field correction, and g is the Kirkwood–Fröhlich correlation factor due to neighboring dipoles. The effective dipole moment, defined as $\mu_{eff} = (g\mu^2)^{1/2}$, was estimated at $\sim 0.95\,D$.

2.5. Pressure–volume–temperature

Literature values were used for the equation of state [27]. The Tait equation was employed

$$V(P,T) = V(0,T)\left\{1 - 0.0894\ln\left[1+\frac{P}{B(T)}\right]\right\} \quad (4)$$

where, $V(0,T) = \exp(-0.307 + 1.859\times10^{-5}T^{3/2})$ (V in cm^3/g, T in Kelvin) is the specific volume at atmospheric pressure and $B(T) = (316.1\text{ MPa})\exp(-0.004078T)$ (T in °C) are the parameters in the melt state. In the glassy state, the following parameters were employed $V(0,T) = (0.8302 + 2.20\times10^{-4}T)$ (V in cm^3/g, T in °C) and $B(T) = (395.4\text{ MPa})\exp(-0.002609T)$ (T in °C).

3. Results and discussion

The components of the dielectric function (ε' and ε'') and of the electric modulus (M' and M'') measured within the temperature range: $421 \le T \le 463$ K are compared in Fig. 1, at the same (reference) temperature ($T_r = 423$ K). In Fig. 1, the frequency axes have been multiplied by appropriate shift factors (a_T) at each T so as to bring the dielectric loss maxima for the segmental (α-) process in coincidence with the dielectric loss maximum of T_r. The vertical axes have also been slightly shifted by corresponding factors b_T and c_T. The horizontal shift factors can be described by the well-known Williams–Landel–Ferry (WLF) equation [20]

$$\log_{10} a_T = -\frac{c^r_{1T}(T-T_r)}{c^r_{2T}+(T-T_r)} \quad (5)$$

where c^r_{1T} and c^r_{2T} are the WLF parameters at the reference temperature. The values of the above parameters at the glass temperature T_g (T_g is operationally defined here as the temperature where the segmental relaxation time is at 1 s) are summarized in Table 1. The constructed "master curves" indicate that tTs works only around the α-process maximum. At higher and lower frequencies, the superposition fails because of the presence of a "fast" β-process and of a "slower" component with distinctly different T-dependencies. The shape of the α-process peak in the ε'' and M'' representations is quite similar with Havriliak–Negami shape parameters of $\alpha = 0.67 \pm 0.07$, $\gamma = 0.5 \pm 0.02$ and $\alpha = 0.6 \pm 0.05$, $\gamma = 0.5 \pm 0.05$, respectively. In the same figure the shifted curves from the shear moduli data (measured within the temperature range $408 \le T \le 463$ K and shifted horizontally with the same shift

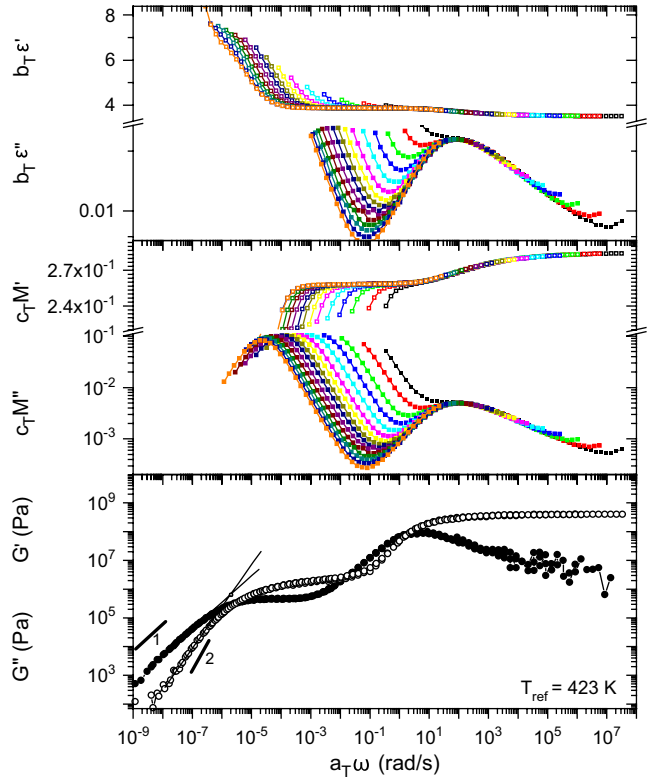

Fig. 1. Comparison of the complex dielectric function (ε^*) with the electric modulus (M^*) and the viscoelastic (shear) moduli (G^*) of BPA-PC at the same reference temperature ($T_r = 423.15$ K). Top: master curve construction using the principle of time–temperature superposition (tTs) for the "isobaric" (at $P = 0.1$ MPa) dielectric permittivity (open symbols) and the dielectric loss (filled symbols) data of ε^*. Middle: master curve construction using tTs for the "isobaric" (at $P = 0.1$ MPa) electric modulus data of the real (open symbols) and imaginary (filled symbols) part of M^*. Bottom: master curve construction using tTs for the storage (open symbols) and loss (filled symbols) shear moduli (G^*) of BPA-PC. Lines with slopes 1 and 2 are drawn, and the range used to define the terminal relaxation times is shown. Notice the good superposition of the rheology data that contrasts with the breakdown of tTs in the ε^* and M^* representations, measured over a broader frequency range.

factors as for the ε^* and M^* representations) are shown at the same reference temperature. Notice that the high-frequency peak in $G''_{\max}$, corresponding to the segmental relaxation, is shifted to lower frequencies as compared to the $\varepsilon''_{\max}$ and $M''_{\max}$ (the latter peak at very similar frequencies due to the low dielectric strength of the segmental process). This suggests that for BPA-PC, dynamic mechanical and dielectric spectroscopies are sensitive to different kinds of motions; the former is sensitive mainly to translational motions of larger entities (i.e., "slow") as opposed to the more localized rotational motions affecting the dielectric response.

The relaxation times for the different processes are compared in Fig. 2. The dielectric relaxation times (filled symbols) are from ($\tau_{M''}$) times with the exception of the slower process where the derivative of the dielectric permittivity was employed. The relaxation times corresponding to the segmental and terminal processes from rheology (open symbols) are also shown for comparison. The relaxation times for the low-temperature β-process display an Arrhenius T-dependence (with HN shape parameters $\alpha = 0.25 \pm 0.05$, $\gamma = 1 \pm 0.05$) that can be described as $\tau_{\max} = \tau_0 \exp(E/kT)$, where $\tau_0 (\sim 1 \times 10^{-14}$ s) is the relaxation time limit at very high T and E is the activation energy (~ 36 kJ/mol). The intensity of the β-process is low ($T\Delta\varepsilon \sim 35$ K), in agreement with earlier studies, however, a detailed investigation of this process is beyond the scope of the current investigation. On the other hand, the segmental process displays the usual strong $\tau(T)$ dependence according to the Vogel–Fulcher–Tammann (VFT) equation

$$\tau_{\max} = \tau_0 \exp\left(\frac{D_T T_0}{T - T_0}\right) \tag{6}$$

where D_T is a dimensionless parameter and T_0 is the "ideal" glass temperature located below T_g ($T_0 = T_g - c^g_{2T}$). Similarly, the slow process in DS displays a VFT dependence (with HN shape parameters $\alpha = 0.85 \pm 0.05$, $\gamma = 1 \pm 0.05$) that can be fitted with the same T_0 parameter as with the corresponding α-process, which implies that both processes freeze at the same temperature. We mention here that this process should

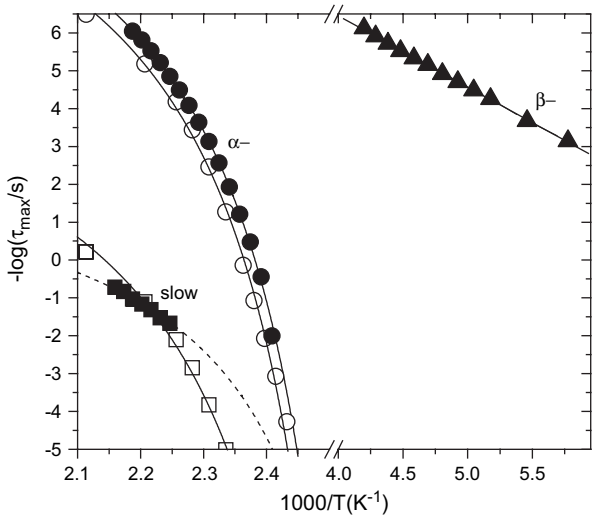

Fig. 2. Arrhenius representation of the relaxation times at maximum loss for the three processes observed in BPA-PC. Three processes are shown: the low-temperature β-process (triangles), the segmental (α-) process associated with the T_g (circles), and a slower process (squares). Filled symbols correspond to the maximum of the electric modulus representation ($\tau_{M''\max}$) of the dielectric data except for the slower process that was obtained from the derivative of the dielectric permittivity. Open symbols correspond to the maximum of the shear loss moduli ($\tau_{G''\max}$) at the segmental and terminal relaxations. The lines are fits to the VFT equation for the slow and α-processes and to the Arrhenius equation for the low-temperature process.

Table 1
VFT parameters of BPA-PC employed for the slow and α-processes by DS and rheology experiments

Technique	Process	τ_0 (s)	D_T	T_0 (K)	T_g (K)	c^g_{1T} (K)	c^g_{2T} (K)
DS	Slow	1.0×10^{-4}	2.1	378	–	–	–
	α-	1.6×10^{-13}	3.2	378	414	15.0	40.4
Rheology	Terminal	1.1×10^{-6}	3.1	381	–	–	–
	α-	5.5×10^{-13}	3.1	381	417	10.4	45.9

not be confused with the ionic motion since it has been derived from the conductivity-free dielectric permittivity. To understand its origin we have undertaken annealing experiments at different temperatures above T_g ($T = T_g + 50$ K and $T = T_g + 100$ K) for different time intervals in 12 h steps. These experiments revealed a decreasing amplitude with annealing time in contrast to that for the segmental process. This suggests that stresses and possible crystallization [28] (not detectable in WAXS) could associate with the dielectric slow process. In addition, notice the different T-dependence of this process with respect to the longest (i.e., terminal) relaxation. The VFT parameters for the segmental and slow process investigated by DS and rheology are summarized in Table 1.

Following the $\tau(T)$ dependence the $\tau(P)$ dependence was investigated and the "isobaric" and "isothermal" results for the relaxation times are depicted in Fig. 3. For the P-dependent times the pressure equivalent of VFT was employed

$$\tau_{max} = \tau_0 \exp\left(\frac{D_P P}{P_0 - P}\right) \quad (7)$$

where D_P is a dimensionless parameter and P_0 is the pressure corresponding to the "ideal" glass transition. The universality of the above equation was tested by plotting the reduced relaxation times as a function of reduced pressure (not shown here) [29]. All relaxation times fall on a single line with zero intercept and slope $D_P = 5.7$.

Of paramount importance in polymer dynamics is the identification of the key parameters that control the segmental dynamics at temperatures near and above T_g [30–35]. According to the simplest "free" volume theory, only density controls the dynamics as opposed to different "landscape" models that emphasize the importance of temperature through the associated thermal energy ($k_B T$). The relative contribution of density and temperature in controlling the segmental dynamics can be addressed through the density representation of the relaxation times as shown in Fig. 4. Knowledge of the equation of state (PVT) allows casting the T- and P-dependencies of the α-relaxation times in a single representation by using the density as the only variable (Fig. 4). In the figure both "the isobaric" (at $P = 0.1$ MPa) and the "isothermal" sets of data (at the seven different temperatures) are shown. The "isothermal" relaxation times can now be described by a modified VFT equation for the density representation as [34,35]

$$\tau_{max} = \tau_\rho \exp\left(\frac{D_\rho \rho}{\rho_0 - \rho}\right) \quad (8)$$

where D_ρ (isothermal: $D_\rho^T = 0.64$ and isobaric: $D_\rho^P = 0.78$) is a dimensionless parameter and ρ_0 is the density at the ideal glass temperature (T_0). The density representation allows for some conclusions with respect to (i) the validity of free-volume theories and (ii) the central parameters controlling glass formation. With respect to (i), the density representation allows access to states with the same density through distinctly different thermodynamic paths obtained by certain T- and P-variations. Under such conditions, a comparison of the iso-density states reveals distinctly different relaxation times. Under the premise that the fractional free volume and the macroscopic volume have a one-to-one correspondence, this last observation contrasts the predictions of even the simplest free-volume theory. We will discuss the central parameters of glass formation with respect to Figs. 6 and 7, below.

The pressure dependence of the "ideal" glass temperature T_0 (or equivalently P_0) and of the normal glass temperature T_g (or P_g) is shown in Fig. 5. The glass-transition temperatures obtained from PVT (open circles) have also been included (a slight shift was necessary to account for the difference in

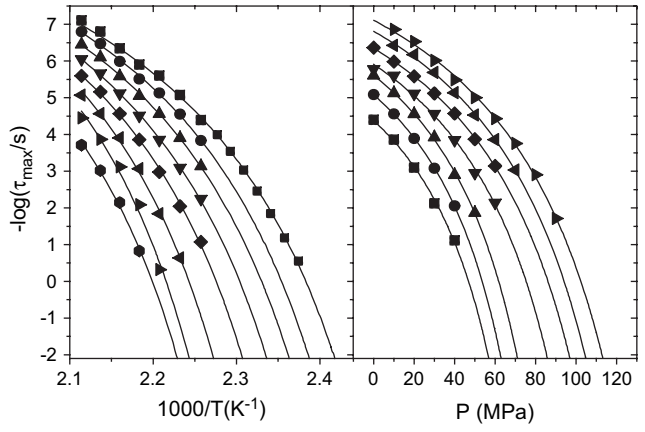

Fig. 3. "Isobaric" (left) and "isothermal" (right) relaxation times corresponding to the α-process M'' maximum of BPA-PC. The different symbols are as follows: for the "isobaric" data: (■) $P = 0.1$ MPa, (●) $P = 10$ MPa, (▲) $P = 20$ MPa, (▼) $P = 30$ MPa, (◆) $P = 40$ MPa, (◀) $P = 50$ MPa, (▶) $P = 60$ MPa, (⬢) $P = 70$ MPa and for the "isothermal" data: (■) $T = 443.15$ K, (●) $T = 448.15$ K, (▲) $T = 453.15$ K, (▼) $T = 458.15$ K, (◆) $T = 463.15$ K, (◀) $T = 468.15$ K, (▶) $T = 473.15$ K. The lines represent the result of the fit of the "isobaric" and "isothermal" data to Eqs. (6) and (7), respectively.

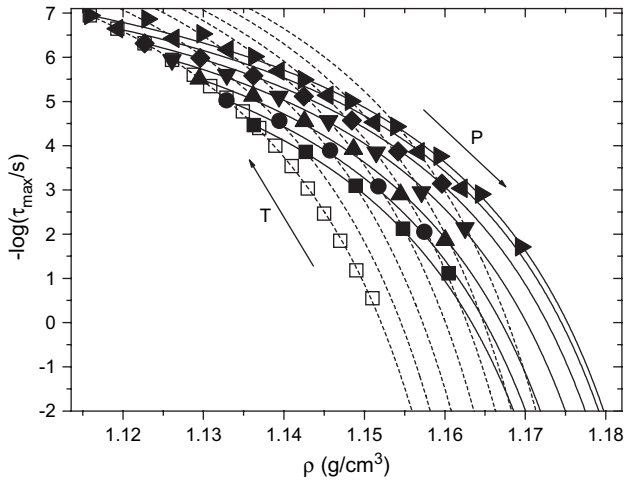

Fig. 4. Dependence of the "isothermal" (solid lines) and "isobaric" (dashed lines) relaxation times on density. The isothermal and isobaric lines are the results of the fits to Eq. (8) with $D_\rho^T = 0.64$ and $D_\rho^P = 0.78$, respectively. The different "isotherms" correspond to the following temperatures: (■) $T = 443.15$ K, (●) $T = 448.15$ K, (▲) $T = 453.15$ K, (▼) $T = 458.15$ K, (◆) $T = 463.15$ K, (◀) $T = 468.15$ K, (▶) $T = 473.15$ K. The "isobaric" data at $P = 0.1$ MPa are shown with open squares.

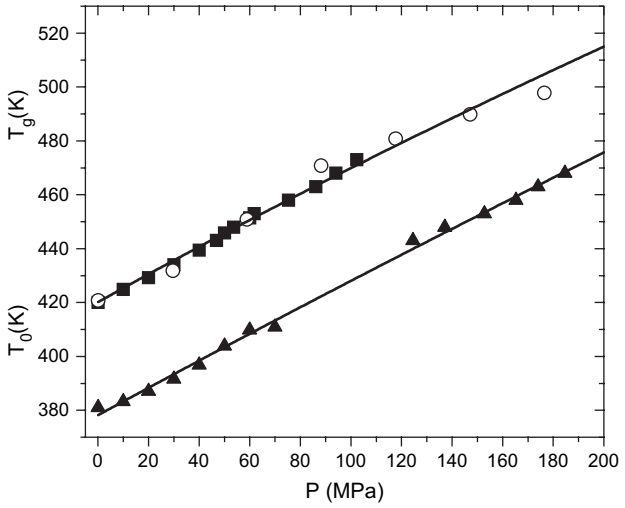

Fig. 5. Pressure dependence of the characteristic temperatures: (○) T_g obtained from PVT measurements [27]; (■) T_g and P_g obtained from "isobaric" and "isothermal" DS relaxation times, respectively (T_g is operationally defined here as the temperature where the segmental relaxation time is at 1 s — this definition brings the T_g in agreement with the PVT results); (▲) T_0 and P_0 values from the VFT fits corresponding to "isobaric" and "isothermal" conditions, respectively. The lines are fits to Eq. (9). Notice the strong T_g (P) and T_0 (P) dependencies.

molecular weights) and are in excellent agreement with the results from the dynamic study. The dependencies have been fitted using the empirical equation first proposed by Simon and Glatzel [36] for the melting of solid gases under pressure

$$T_0(P) = c\left(1 + \frac{b}{a}P\right)^{1/b} \tag{9}$$

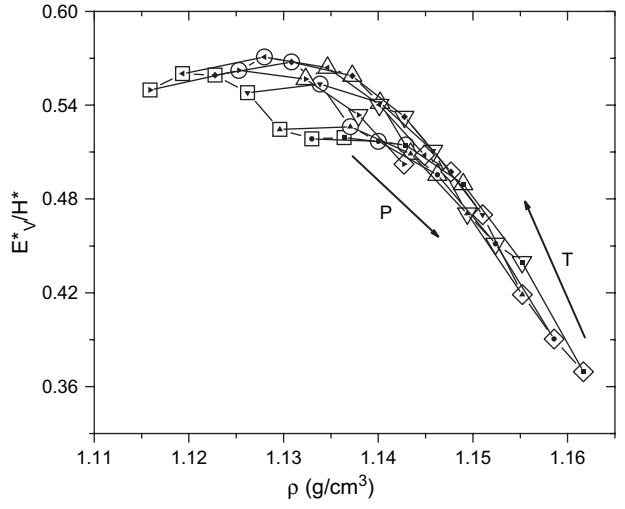

Fig. 6. Ratio of the constant-volume activation energy (E_V^*) to the enthalpy of activation (H^*) plotted against density obtained at the crossing points of Fig. 4 using Eq. (10). The arrows show the direction of increasing temperature and pressure for the "isobaric" and "isothermal" sets, respectively. The "isothermal" data are at (■) $T = 443.15$ K, (●) $T = 448.15$ K, (▲) $T = 453.15$ K, (▼) $T = 458.15$ K, (◆) $T = 463.15$ K, (◀) $T = 468.15$ K, (▶) $T = 473.15$ K and the "isobaric" data are at: (□) $P = 0.1$ MPa, (○) $P = 10$ MPa, (△) $P = 20$ MPa, (▽) $P = 30$ MPa, (◇) $P = 40$ MPa.

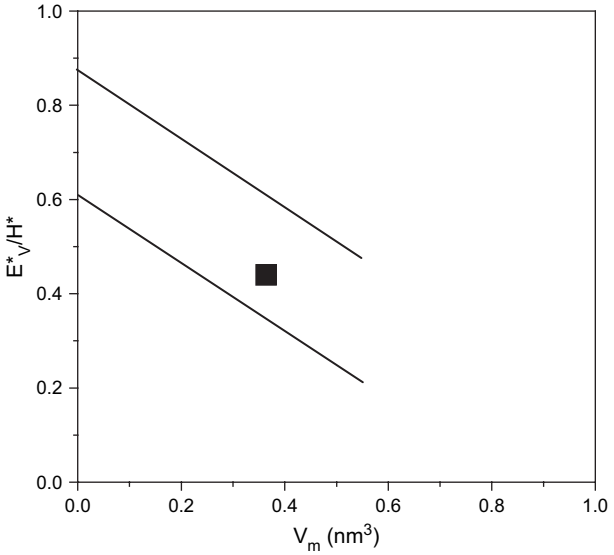

Fig. 7. Ratio of the constant-volume activation energy (E_V^*) to the enthalpy of activation (H^*) plotted as a function of the monomer volume. The lines (with slope of −0.72) delineate the region in $E_V^*/H^* - V_m$ space formed by 27 glass-forming systems (18 polymers and 9 small molecules). The symbol corresponds to BPA-PC at $P = 0.1$ MPa and $T = T_g(\tau \sim 1$ s).

where c is the glass temperature at ambient pressure ($P = 0.1$ MPa) and b, a are polymer specific parameters. For $\tau = 1$ s (filled squares) these parameters are $c = T_g(0) = 420$ K, $b = 1.97$ and $a = 799$ MPa and for $\tau \to \infty$ (filled triangles): $c = T_0(0) = 378$ K, $b = 1.39$ and $a = 740$ MPa. From the initial slopes of these curves we obtain $(dT_g/dP)_{P\to 0}$ values of 0.52 K/MPa and 0.51 K/MPa for $\tau = 1$ s and $\tau \to \infty$, respectively. Notice the unusually high pressure coefficient for BPA-PC that may reflect the packing irregularities found in PALS [10,11].

The role of temperature and density in the glass-transition dynamics of glass formers can be obtained by calculating the activation energy at constant density or volume $E_V^* = -RT^2(\partial \ln \tau_{max}/\partial T)_V$ and the enthalpy of activation as $H^* = -RT^2(\partial \ln \tau_{max}/\partial T)_P$. The ratio E_V^*/H^* lies in the range 0−1; a value of zero indicates that density is the main controlling parameter of the dynamics, whereas a value near one suggests temperature and the associated thermal energy as the controlling parameter, instead. These possibilities should be seen only as extreme cases since even in the case of thermally activated processes, the potential energy barriers will also depend on the local density [37]. It can be readily shown that the ratio E_V^*/H^* can be expressed as [35]

$$\frac{E_V^*}{H^*} = 1 - \frac{\left(\dfrac{\partial \ln \tau_{max}}{\partial \rho}\right)_T}{\left(\dfrac{\partial \ln \tau_{max}}{\partial \rho}\right)_P} \tag{10}$$

which permits its calculation from the density representation (Fig. 4) without any extrapolations. The thus-obtained values of the ratio E_V^*/H^* for the different (T,P) conditions are plotted in Fig. 6 as a function of density. As seen in that figure, the

ratio assumes values in the range 0.36–0.57 under the different (T,P) conditions investigated. For BPA-PC, at $T = T_g$ (i.e., $\tau \sim 1$ s) and $P = 0.1$ MPa, the ratio assumes values in the vicinity of 0.42 ($\rho = 1.155$ g/cm^3). The same ratio can be calculated independently from Ref. [30]

$$\frac{E_V^*}{H^*} = 1 - \left(\frac{\partial P}{\partial T}\right)_V \left(\frac{\partial T}{\partial P}\right)_\tau \tag{11}$$

where $(\partial P/\partial T)_V$ can be obtained from the equation of state and $(\partial T/\partial P)_\tau$ is the pressure coefficient of T_g. Using $(\partial P/\partial T)_{V|\tau=1\ s} = 1.079$ MPa/K, and $(\partial T/\partial P)_{\tau=1\ s} = (\partial T_g/\partial P)_{P\to 0} = 0.52$ K/MPa, we obtain a value of 0.44 ($\tau \sim 1$ s, $P = 0.1$ MPa).

In addition, Ferrer et al. [38], have shown that the same ratio can be obtained from the ratio of the isobaric $\alpha_P = (\partial \ln V/\partial T)_P$ to the isochronic $\alpha_\tau = (\partial \ln V/\partial T)_\tau$ thermal expansion coefficients as

$$\frac{E_V^*}{H^*} = \frac{1}{1 - \dfrac{\alpha_P}{\alpha_\tau}} \tag{12}$$

In Eq. 12, α_P is determined directly from the PVT measurements at $T > T_g$, whereas the isochronic thermal expansion coefficient can be obtained from $\alpha_\tau = \mathrm{d}(\ln V(T_g))/\mathrm{d}T_g(P)$. The thus-obtained ratio amounts to 0.46 in agreement with the earlier estimations.

The value of the ratio E_V^*/H^* ($\sim$0.44) is among the lowest reported for a polymeric substance indicating the significance of density in controlling the segmental dynamics of BPA-PC on approaching T_g. Recently [39], a correlation was demonstrated between this dynamic quantity and the monomeric volume ($V_m = M/\rho N_A$, where M is the monomer molecular weight) for 27 glass formers (polymers and glass-forming liquids). This is schematically depicted in Fig. 7 by the region between the parallel lines together with the location of BPA-PC. Flexible polymers with small side chains and of low V_m exhibit high values of the dynamic ratio signifying the importance of temperature through the intra-molecular degrees of freedom [39]. On the other hand, polymers with bulky side chains or large monomeric volumes exhibit lower values for the dynamic quantity suggesting the increasing importance of density and packing on the segmental dynamics [39]. In extreme cases of very large monomeric volumes this suggests that the free volume is the controlling parameter of the liquid-to-glass dynamics. Likewise, for the extreme case of very small monomeric volumes and flexible main-chain polymers free volume is unimportant and the dynamics are solely controlled by the thermal energy required to explore the energy landscape. For intermediate cases of monomeric volumes, both density and temperature are controlling the dynamics. In BPA-PC the segmental dynamics in the vicinity of T_g are largely controlled by density due to the large monomeric volume. These results for the dynamics are in agreement with the findings from PALS suggesting a defect-full polymer with a high fractional free volume at T_g. These packing irregularities are responsible for the low values of the dynamic ratio E_V^*/H^* and possibly for the high pressure coefficient of T_g.

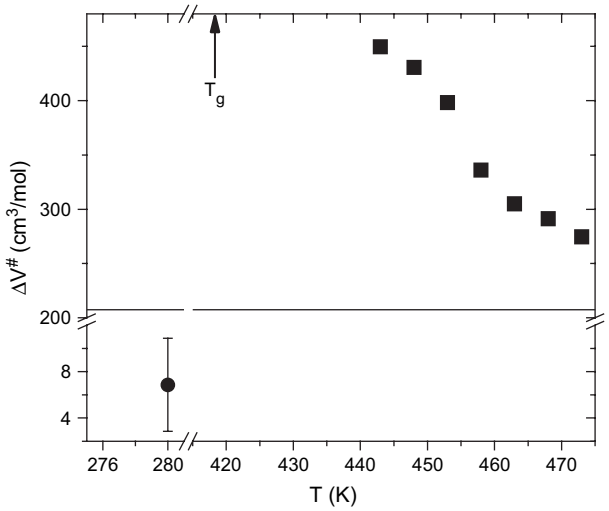

Fig. 8. Apparent activation volume, $\Delta V^\#$, as a function of temperature for the α- (■) and the faster (β-) (●) processes of BPA-PC. Note that the apparent activation volume corresponding to the α-process approaches the monomer volume ($V_m = 207$ cm^3/mol shown with the solid line) at high temperatures and increases rapidly by decreasing T toward T_g. Note the very low $\Delta V^\#(T)$ value for the β-process.

Notice that this approach based on the monomeric volume [39] is very different from the proposed thermodynamic scaling for the segmental relaxation times as $\log \tau \sim T^{-1}\rho^x$ [31–33], where x is a material constant, or $\ln \tau \sim (\rho - \rho^*)T^{-1}$ [40,41] that despite their appealing forms lack a predictive power.

From the initial slope of the ''isothermal'' lines of Fig. 3, the apparent activation volume, $\Delta V^\#$, can be obtained as

$$\Delta V^\# = \mathrm{R}T\left(\frac{\partial \ln \tau_{max}}{\partial P}\right)_T \tag{13}$$

originally interpreted as reflecting the difference in molar volume of activated and non-activated species. The temperature dependence of this quantity is shown in Fig. 8. Recent experiments revealed that $\Delta V^\#$: (i) scales with the temperature difference from T_g for homopolymers of varying molecular weights [42,43,35], (ii) shows a strong T-dependence, increasing by decreasing T, and (iii) approaches the monomer volume ($\Delta V = 207$ cm^3/mol) some 70 K above T_g. The apparent activation volume of the β-process was also estimated as $\sim$6 cm^3/mol. The latter value is in agreement with earlier estimates based on pressure-dependent NMR [15,16]. According to these earlier ^{2}H spin-lattice relaxation experiments, the β-process as seen by NMR, is attributed to three processes; π-phenylene flips, small-angle fluctuations about the flip axes and wiggling about the axes perpendicular to the rings. The small activation volume suggested that the motion is highly restricted and that large volume fluctuations can be excluded at least at low temperatures.

4. Conclusions

Pressure-dependent dielectric spectroscopy is employed to shed light on the origin of the liquid-to-glass transition of

bisphenol-A-polycarbonate. The temperature and pressure dependence of the segmental relaxation times coupled to the equation of state revealed that:

(i) The segmental dynamics are controlled both by density and temperature. However, on approaching T_g, molecular packing and density have a stronger influence on the dynamics than temperature. This is documented by independent calculations (from the equation of state and from the $\tau(T)$ and $\tau(P)$ dependencies) of the activation ratio E_V^*/H^* at T_g. Clearly intra-molecular conformational dynamics alone cannot account for the segmental dynamics in BPA-PC. The value of E_V^*/H^* at T_g is discussed in terms of a recent study relating the activation ratio to the monomeric volume. The low value of this ratio originates from the large monomeric volume of BPA-PC.
(ii) The pressure coefficient of T_g is one of the highest for a polymer substance (0.52 K/MPa).
(iii) The apparent activation volume for the α-process has a steep T-dependence and approaches the monomer volume at higher temperatures. The corresponding quantity for the low-temperature γ-process was much smaller than the monomer volume in agreement with earlier estimations.

Acknowledgments

We thank Mr. George Tsoumanis for technical support at the UoI. This work was supported by the GSRT grants PENED 01ED529 and 03ED856.

References

[1] Schaefer J, Stejskal EO, Perchak D, Skolnick J, Yaris R. Macromolecules 1985;18:368.
[2] Jones AA. Macromolecules 1985;18:902.
[3] Fischer EW, Hellmann GP, Spiess HW, Hörth F-J, Ecarius U, Wehrle M. Macromol Chem Suppl 1985;12:189.
[4] Yee AF, Smith SA. Macromolecules 1981;14:54.
[5] Ngai KL, Rendell RW, Yee AF. Macromolecules 1988;21:3396.
[6] Floudas G, Higgins J, Meier G, Kremer F, Fischer EW. Macromolecules 1993;26:1676.
[7] Katana G, Kremer F, Fischer EW, Plaetschke R. Macromolecules 1993;26:3075.
[8] Merenga AS, Papadakis CM, Kremer F, Liu J, Yee AF. Macromolecules 2001;34:76.
[9] Eilhard J, Zirkel A, Tschöp W, Hahn O, Kremer F, Schärpf O, et al. J Chem Phys 1999;110:1819.
[10] Kluin J-E, Yu Z, Vleeshouwers S, McGervey JD, Jamieson AM, Simha R. Macromolecules 1992;25:5089.
[11] Kristiak J, Bartos J, Kristiakova K, Sausa O, Bandzuch P. Phys Rev B 1994;49:6601.
[12] Cangialosi D, Wübbenhorst M, Schut H, van Veen A, Picken SJ. Phys Rev B 2004;69:134206.
[13] Thurau CT, Ediger MD. J Chem Phys 2003;118:1996.
[14] Leon S, van der Vegt N, Delle Site L, Kremer K. Macromolecules 2005;38:8078.
[15] Walton JH, Lizak MJ, Conradi MS, Gullion T, Schaefer J. Macromolecules 1990;23:416.
[16] Hansen MT, Kulik AS, Prins KO, Spiess HW. Polymer 1992;33:2231.
[17] Floudas G. Broadband dielectric spectroscopy. In: Kremer F, Schönhals A, editors. Berlin: Springer; 2002 [chapter 8].
[18] Floudas G. Prog Polym Sci 2004;29:1143.
[19] Roland CM, Hensel-Bielowka S, Paluch M, Casalini R. Rep Prog Phys 2005;68:1405.
[20] Ferry JD. Viscoelastic properties of polymers. 3rd ed. New York: Wiley; 1980.
[21] Bendler JT, Fontanella JT, Shlesinger MF. Phys Rev Lett 2001;87:195503.
[22] Angell CA. Science 1995;267:1924.
[23] Stillinger FH. Science 1995;267:1935.
[24] Floudas G, Pakula T, Stamm M, Fischer EW. Macromolecules 1993;26:1671.
[25] Wübbenhorst M, van Koten E, Jansen J, Mijw M, van Turnhout J. Macromol Rapid Commun 1997;18:139.
[26] Moynihan CT. Solid State Ionics 1998;105:175.
[27] Zoller P. J Polym Sci Polym Phys Ed 1982;20:1453.
[28] van Asten AC, Kok WT, Tijssen R, Poppe H. J Polym Sci Polym Phys Ed 1996;34:283.
[29] Paluch M, Patkowski A, Fischer EW. Phys Rev Lett 2000;85:2140.
[30] Naoki M, Endou H, Matsumoto K. J Phys Chem 1987;91:4169.
[31] Tölle A, Schober H, Wuttke J, Randl OG, Fujara F. Phys Rev Lett 1998;80:2374.
[32] Casalini R, Roland CM. Phys Rev E 2004;69:062501.
[33] Roland CM, Paluch M, Pakula T, Casalini R. Philos Mag 2004;84:1573.
[34] Mpoukouvalas K, Floudas G. Phys Rev E 2003;68:031801.
[35] Papadopoulos P, Peristeraki D, Floudas G, Koutalas G, Hadjichristidis N. Macromolecules 2004;37:8116.
[36] Simon FE, Glatzel G. Z Anorg Allg Chem 1929;178:309.
[37] Pakula T. J Mol Liq 2000;86:109.
[38] Ferrer M-L, Lawrence C, Demirjian BG, Kivelson D, Alba-Simionesco C, Tarjus G. J Chem Phys 1998;109:8010.
[39] Floudas G, Mpoukouvalas K, Papadopoulos P. J Chem Phys 2006;124:074905.
[40] Alba-Simionesco C, Cailliaux A, Tarjus G. Europhys Lett 2004;68:58.
[41] Dreyfus C, Le Grand A, Gapinski J, Steffen W, Patkowski A. Eur Phys J B 2004;42:309.
[42] Floudas G, Gravalides C, Reisinger T, Wegner G. J Chem Phys 1999;111:9847.
[43] Mpoukouvalas K, Floudas G, Zhang SH, Runt J. Macromolecules 2005;38:552.